Kovove Mater. 52 2014 47–55
DOI: 10.4149/km_2014_1_47

The solution and aging behavior of Mg-8Li-3Al-xCe(x = 0, 1.0) alloys

Huayi Lin, Ruizhi Wu*, Pengfei Fei, Zhe Leng, Xuying Guo, Jinghuai Zhang, Bin Liu, Milin Zhang

Key Laboratory of Superlight Materials & Surface Technology, Ministry of Education, Harbin Engineering University, Harbin 150001, P. R. China

Received 11 September 2013, received in revised form 23 September 2013, accepted 23 September 2013

Abstract

The microstructure and microhardness properties of the as-cast, as-soluted and as-aged alloys of Mg-8Li-3Al-xCe(x = 0, 1.0) were investigated. The as-cast Mg-8Li-3Al (LA83) alloy consists of α-Mg, β-Li, AlLi and $MgLi_2Al$ phases. The as-cast LA83-1Ce alloy consists of α-Mg, β-Li, $MgLi_2Al$, AlCe and Al_2Ce phases. Besides, the addition of Ce can refine and spheroidize the microstructure of as-cast LA83 alloy. After the addition of Ce, the HV of α and β phases were improved by 137 % and 127 %, respectively, and the HV value difference between α and β became small. Heat treatment can raise the alloy-HV, α-HV and β-HV of LA83 and LA83-1Ce alloys. The variation in hardness during aging process is attributed to the precipitation of $MgLi_2Al$ phase and the possibility of the transformation from AlLi phase to $MgLi_2Al$ phase. With the increase of aging temperature, the size of $MgLi_2Al$ phase becomes larger apparently, causing the age softening phenomenon happens.

K e y w o r d s: Mg-Li alloy, Ce, aging behavior microhardness, microstructure

1. Introduction

In the 21st century, with the higher requirement of lightweight in modern industry, Mg-Li alloys have drawn increasing attentions, due to their low density and high specific strength, in aerospace, nuclear industry, ordnance industry and other fields [1–4].

According to the Mg-Li phase diagram, Mg-Li alloys exhibit two phase structures between 5.7 and 10.3 mass% Li contents consisting of the Li-rich BCC--structured β phase and the Mg-rich HCP-structured α phase at room temperature [5, 6]. To improve the mechanical properties of Mg-Li alloy, the addition of alloying elements (such as aluminum, zinc, etc.), heat treatment and deformation are the major methods [7, 8]. The addition of Ce results in the solid solution of Ce in matrix and the formation of AlCe and Al_2Ce phases, ensuring the effects of solution strengthening and secondary phase strengthening [9, 10]. To refine the grain of alloys, Ce is often added in magnesium alloys in previous citations. The suitable Ce content in Mg-Li alloys is l % (mass fraction). It is well known that precipitation occurs in solid-solution treated MgLiAl/Zn alloys during aging at room temperature. Initially, hardness is enhanced by the precipitates. With further aging, hardness decreases monotonically [11, 12]. It is generally believed that the age-hardening phenomena of Mg-Li-Al connects with a metastable phase called θ ($MgLi_2Al$). However, θ ($MgLi_2Al$) is unstable and finally transforms to stable AlLi phase [13–15].

Aging behavior of Mg-Li-Al alloys has long been investigated [16–20]. However, few studies have been carried out to examine the effect of Ce on aging behavior. In this paper, the changes of microstructure and microhardness of Mg-8Li-3Al-xCe(x = 0, 1.0) alloys were studied. The relationship between microstructure and heat treatment behavior was analyzed to explore the strengthening mechanisms.

2. Experimental method

Mg-8Li-3Al-xCe(x = 0, 1.0) were prepared from

*Corresponding author: tel.: +86-451-82569890; fax: +86-451-82569890; e-mail address: Ruizhiwu2006@yahoo.com

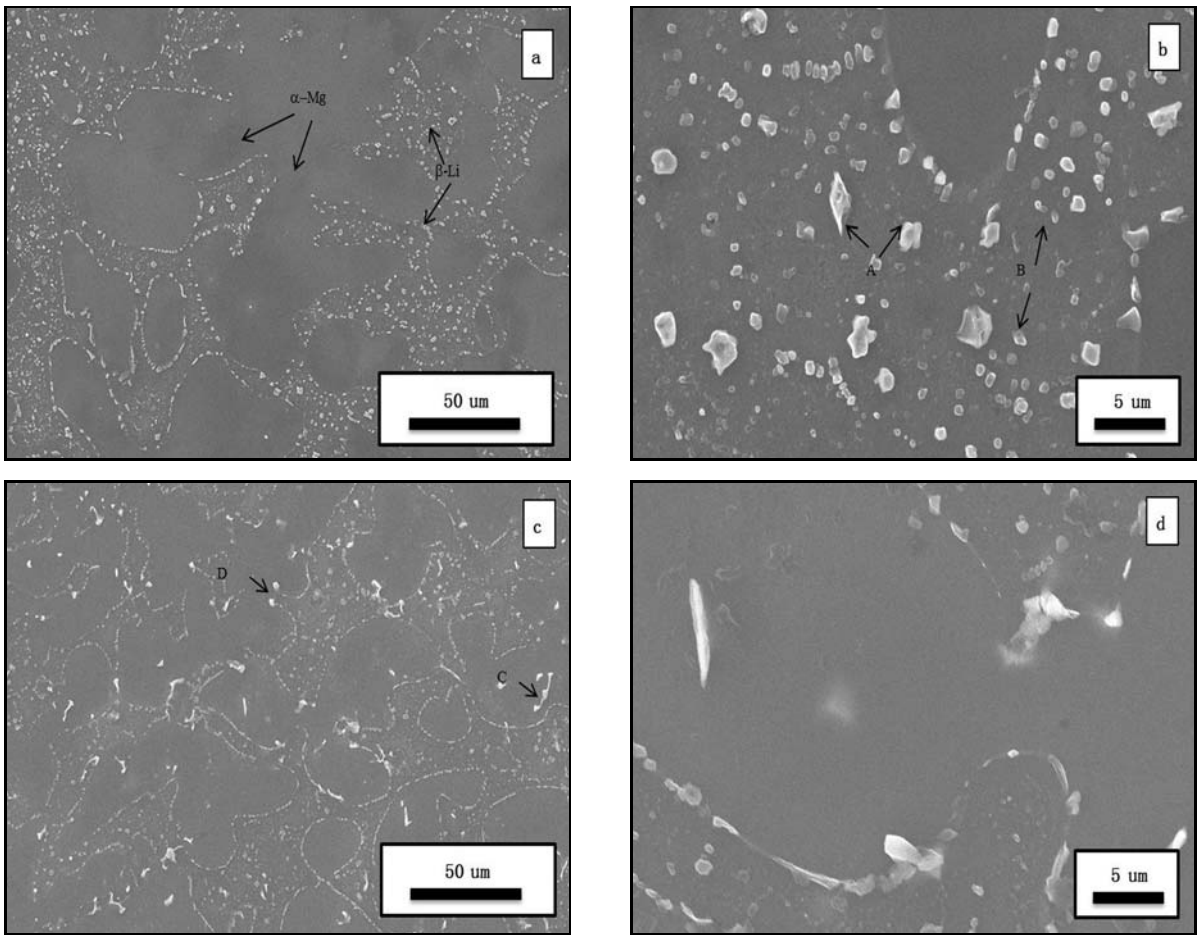

Fig. 1. SEM images of the as-cast LA83-xCe alloy: (a) – (b) LA83 alloy, (c) – (d) LA83-1Ce.

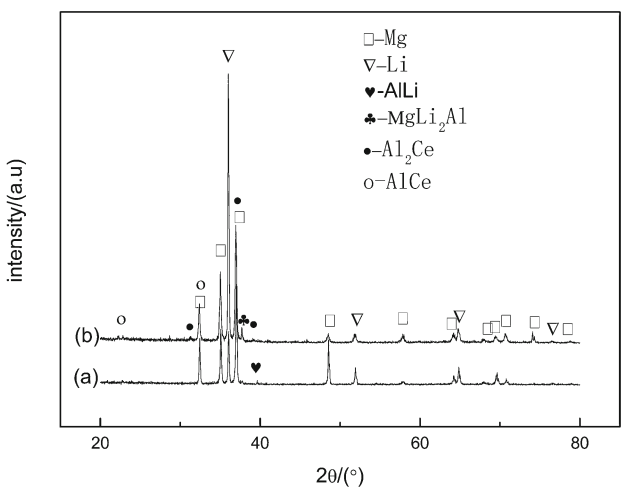

Fig. 2. The XRD patterns of as-cast LA83-xCe alloys: (a) $x = 0$, (b) $x = 1$.

commercial pure Mg, Li, Al and Mg-20.6wt.%Ce master alloy. Under an anti-oxidizing protective atmosphere of pure argon, the alloys were melted in an induction furnace with a low carbon steel crucible. The melt was cast into a 125 mm × 37 mm steel mold. Then the specimens with dimensions of 10 mm × 10 mm × 10 mm were cut from as-cast ingots. The solution treatment was carried at 300 ℃ for 0–2 h. All heat-treated samples were quenched in the water with room temperature. The LA83 alloy after solution (300 ℃ × 1 h) was then aged at room temperature, 50 ℃, 100 ℃, 150 ℃, 200 ℃ for 1 h. The LA83-1Ce alloy after solution (300 ℃ × 2 h) was aged at room temperature, 50 ℃, 100 ℃, 150 ℃, 200 ℃ for 1 h.

The specimens for microstructure observation were prepared by conventional metallographic techniques. Then they were etched for 10–20 s with a solution of 2 vol.% nitric acid in alcohol before observation. The microstructure was observed by scanning electron microscopy (SEM) equipped with energy dispersive spectrometer (EDS). Phase identification was performed using an X-ray diffractometer with Cu Kα radiation at 40 kV and 150 mA. The hardness was measured with microhardness tester according to the standard of GB/T4340.1-2009 [21]. The HV of the alloys was measured with the microhardness tester. When measuring the HV of the alloys, the load was 1000 gf and the holding time was 30 s. When measuring the HV

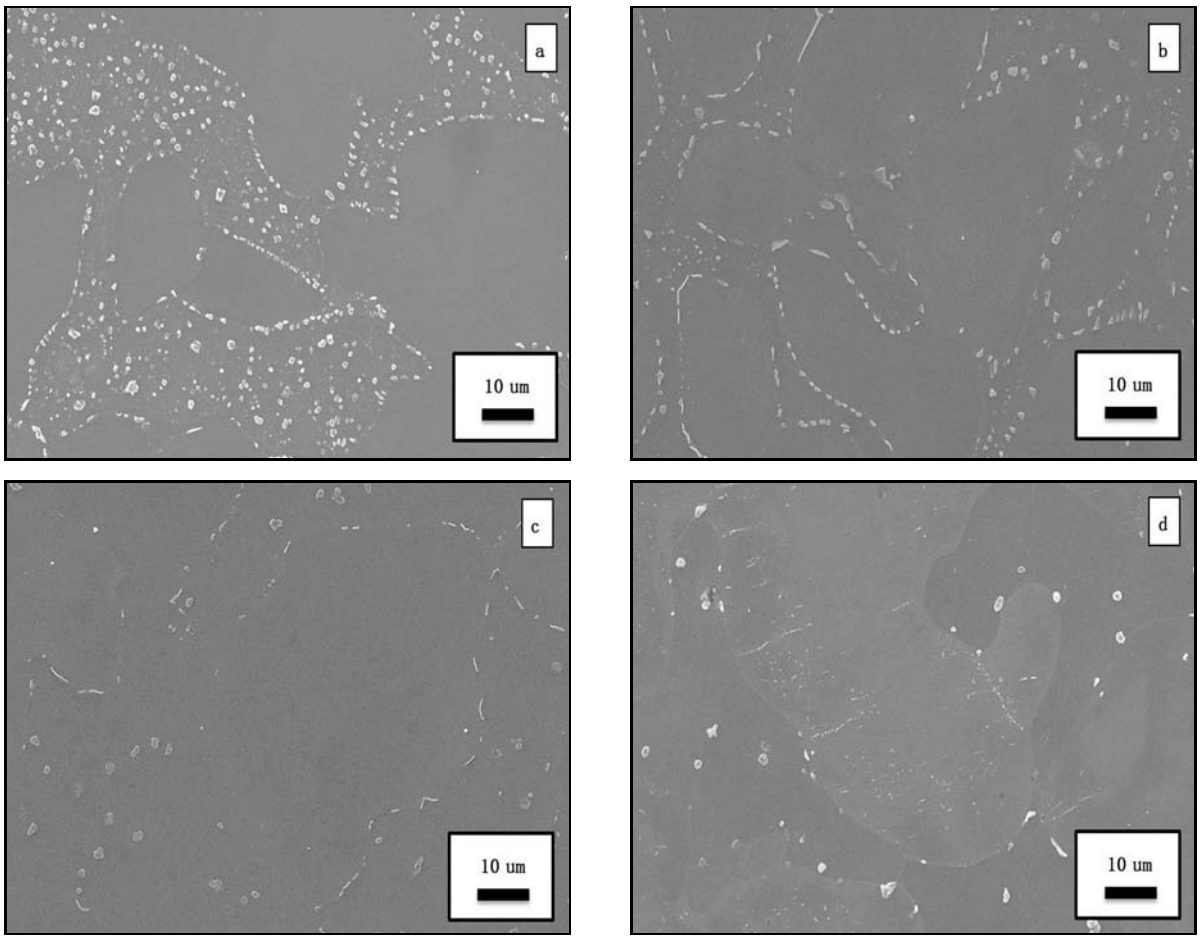

Fig. 3. SEM images of LA83 alloy after solution treatment at 300 ℃ from 0 h to 2 h: (a) 0 h, (b) 0.5 h, (c) 1 h, (d) 2 h.

of α and β phases, the load was 10 gf and the holding time was 10 s. The hardness values reported in this paper are the average of five measurements.

3. Results and discussion

3.1. Analysis of the microstructure

3.1.1. Analysis of the microstructure of as-cast LA83 and LA83-1Ce alloys

Figure 1 shows the SEM images of LA83-xCe as--cast alloys. It reveals that LA83 alloy is mainly composed of α-Mg and β-Li. The shape of α phase is round-like, and there exist many particles inside the β phase, as shown in Fig. 1a. Figure 1b shows the SEM image of as-cast LA83 alloy in high magnification case. There are two sizes of particles inside the β phase matrix, namely, some large particles (marked as A) and fine particles (marked as B). The size of the former is from 1.17 μm to 4.61 μm, and the size of the latter is less than 1 μm.

After the addition of Ce, A particles disappear in Fig. 1d, and the amount of B particles inside the β phase gradually decreases. Besides, the size of B particles becomes smaller. Moreover, with the addition of Ce, a great number of long strip morphology phase (marked as C) form and distribute in the α-β boundary region and α phase as seen in Fig. 1c, and round morphology phase (marked as D) is observed in Fig. 1c. The existence of C and D refines and spheroidizes the microstructure.

The XRD diffraction patterns of as-cast LA83--xCe(0, 1.0) alloy are illustrated in Fig. 2. It indicates that the as-cast LA83 alloy consists of α-Mg, β-Li, $MgLi_2Al$ and AlLi phases. AlCe and Al_2Ce appear in the Mg-8Li-3Al-1Ce alloy. Combining XRD analysis and SEM microstructure, it can be deduced that points of C and D in Fig. 1 generated after Ce addition are AlCe/Al_2Ce compounds. The electronegative difference between Ce and Al is 0.4, while that between Mg and Al is 0.1. Taking this into account, it can be known that Al and Ce form compounds preferentially. In LA83-1Ce, besides α phase and β phase, there exists $MgLi_2Al$ phase. Thus, it can be judged that the A particles inside β-phase are AlLi phase.

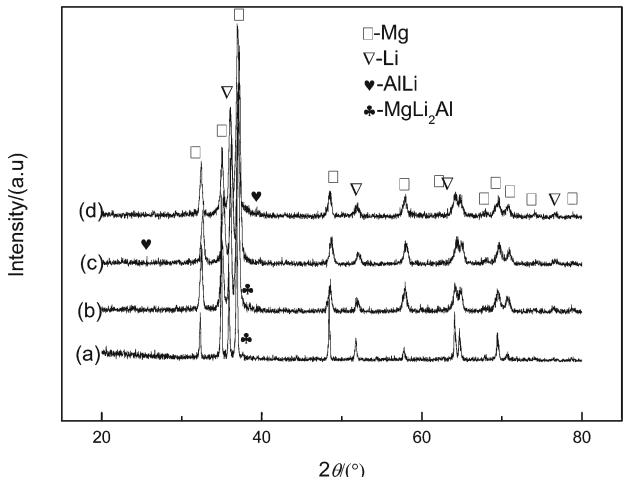

Fig. 4. The XRD patterns of LA83 alloy after solution treatment at 300 ℃ from 0 h to 2 h: (a) 0 h, (b) 0.5 h, (c) 1 h, (d) 2 h.

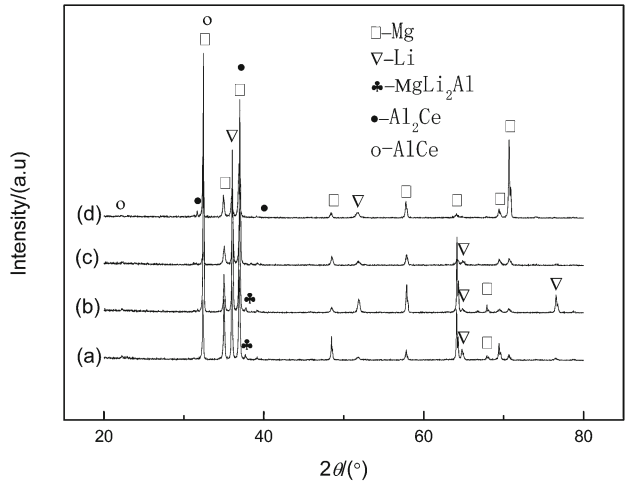

Fig. 6. The XRD patterns of LA83-1Ce alloy after solution treatment at 300 ℃ from 0 h to 2 h: (a) 0 h, (b) 0.5 h, (c) 1 h, (d) 2 h.

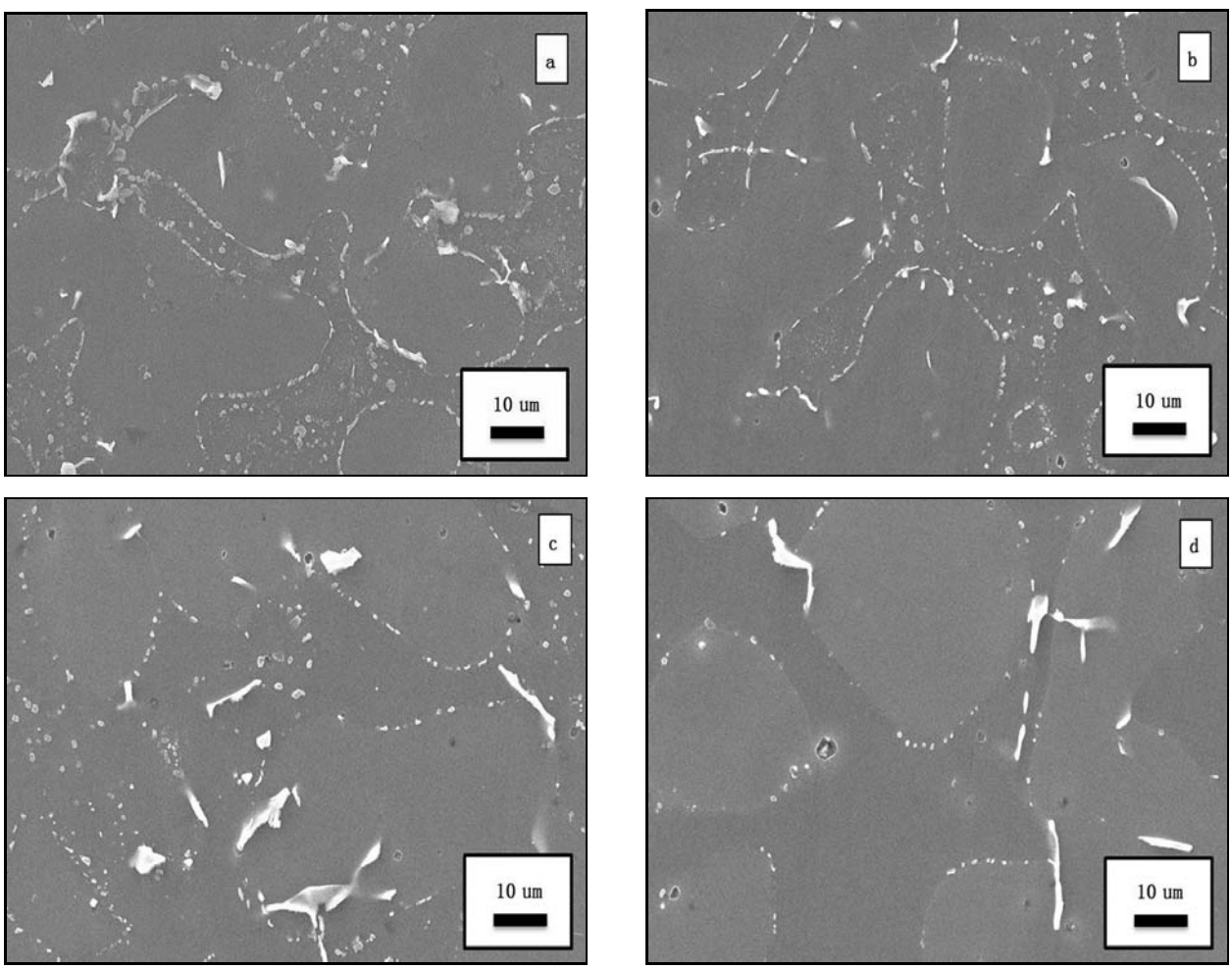

Fig. 5. SEM images of LA83-1Ce alloy after solution treatment at 300 ℃ from 0 h to 2 h: (a) 0 h, (b) 0.5 h, (c) 1 h, (d) 2 h.

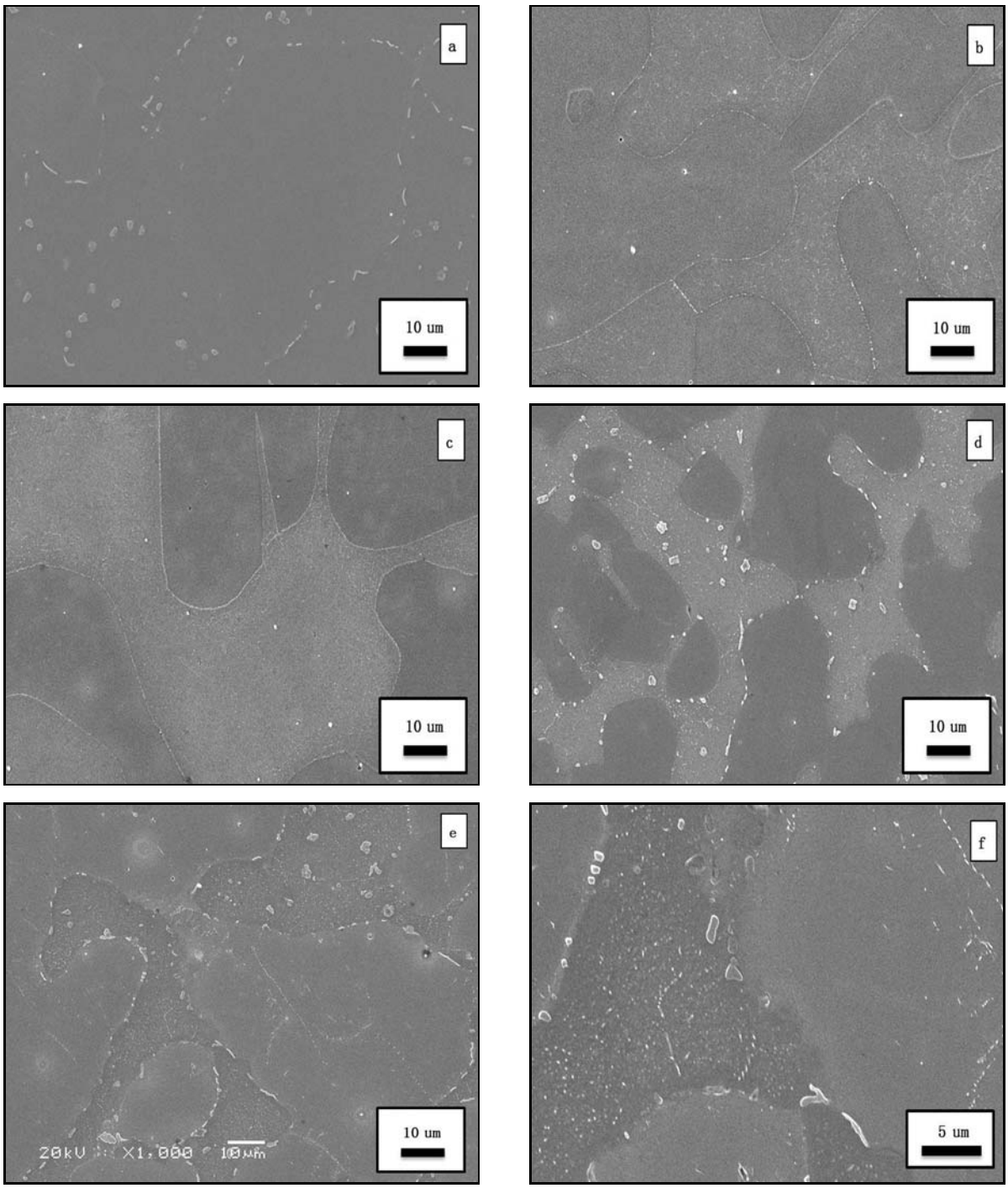

Fig. 7. SEM images of LA83 alloy aged for 1 h at different temperatures: (a) room temperature, (b) 50 ℃, (c) 100 ℃, (d) 150 ℃, (e) – (f) 200 ℃.

3.1.2. Analysis of the microstructure of as-soluted LA83 and LA83-1Ce alloys

Figure 3 shows the SEM images of LA83 after solution treatment at 300 ℃ for 0–2 h. Figure 4 shows XRD results of LA83 alloy after solution treatment at 300 ℃ for 0–2 h. The results show that, after solution treatment, most of $MgLi_2Al$ phases are solutionized into the matrix, and the residual AlLi phase exists in β phase, as shown in Fig. 3c,d. Besides, the shape of AlLi phase transforms from the irregular shape to the round shape. After solution at 300 ℃ for 2 h, the α-β phase boundaries regions of LA83 alloys become clear, without the existence of $MgLi_2Al$ phase. Combining XRD analysis and microstructure, it can be deduced that fine lamellae in α-Mg and large particles in β-Li

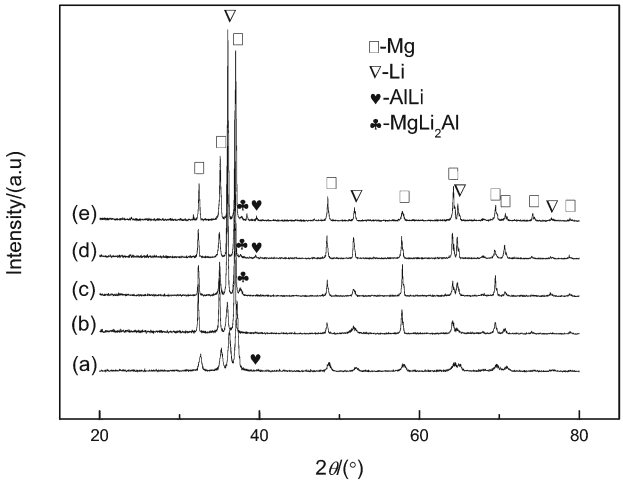

Fig. 8. XRD patterns of LA83 alloy aged for 1 h at different temperatures: (a) room temperature, (b) 50 ℃, (c) 100 ℃, (d) 150 ℃, (e) 200 ℃.

are AlLi phase, as demonstrated in Fig. 4d.

Figure 5 shows the SEM images of LA83-1Ce alloy after solution treatment at 300 ℃ for 0–2 h. Figure 6 shows XRD results of LA83-1Ce alloy after solution treatment at 300 ℃ for 0–2 h. The $MgLi_2Al$ phase is solutionized into the matrix with the increase of solution time, shown as Fig. 6. The AlCe and Al_2Ce phases still exist in the solution-treated alloy because of their good thermal stability.

3.1.3. Analysis of aging behavior of LA83 and LA83-1Ce alloys

Figure 7 shows SEM images of LA83 alloy which was heated at 300 ℃ for 1 h and then aged for 1 h at room temperature, 50 ℃, 100 ℃, 150 ℃, 200 ℃, respectively. Figure 8 shows XRD patterns of LA83 alloy which was solution treated at 300 ℃ for 1 h and aged for 1 h at room temperature, 50 ℃, 100 ℃, 150 ℃, 200 ℃, respectively. When aging temperature increases to 50 ℃, large quantity of $MgLi_2Al$ phases in β matrix are found, AlLi phases are not found in matrix. It was found that, there is no $MgLi_2Al$ peak in the XRD pattern for the specimen aged for 1 h at 50 ℃ because the amount of $MgLi_2Al$ is too low to detect. With the increase of aging temperatures, the amount of $MgLi_2Al$ increases and the size of precipitate becomes larger, which is coordinate with the $MgLi_2Al$ diffraction peak in Fig. 8. When aging temperature increases to 150 ℃ and 200 ℃, large quantity of AlLi phases in β matrix are found, which are coordinate with the AlLi diffraction peak in Fig. 8.

Figure 9 shows SEM images of LA83-1Ce alloy which was heated at 300 ℃ for 1 h and then aged for 1 h at room temperature, 50 ℃, 100 ℃, 150 ℃, 200 ℃. Figure 10 shows XRD patterns of LA83-1Ce alloy which was solution treated at 300 ℃ for 1 h and aged for 1 h at room temperature, 50 ℃, 100 ℃, 150 ℃, 200 ℃, respectively. It was found that there was no $MgLi_2Al$ peak in the XRD pattern for the specimen aged for 1 h at 50 ℃ and 100 ℃. When aging temperature increases to 150 ℃, large quantity of fine $MgLi_2Al$ phases in β matrix are found, which is coordinated with the $MgLi_2Al$ diffraction peak in Fig. 10. When aging temperature increases to 200 ℃, the amount of $MgLi_2Al$ increases and the size of $MgLi_2Al$ becomes larger, which is coordinated with the $MgLi_2Al$ diffraction peak in Fig. 8. It was found that there is no AlLi peak in the XRD pattern in aging process.

3.2. Comparison of microhardness

3.2.1. Comparison of the hardness of as-cast LA83 and LA83-1Ce alloys

Figure 11 plots the alloy-HV, α-HV and β-HV of the as-cast Mg-8Li-3Al-xCe($x = 0, 1.0$) alloys. It is observed that the addition of Ce improves the HV of α and β phases, and the alloy-HV of as-cast LA83 alloy. Besides, the HV value difference between α and β becomes closer. It is well known that Ce has a small solid solubility in magnesium [22]. With the addition of Ce, AlCe and Al_2Ce form, and they mainly distribute in the α-β boundaries regions and α phase, refining and spheroidizing the microstructure, increasing the HV of α and β phases. The effects of solution strengthening, Al weakening and microstructure refinement result in the small change of the HV of as-cast LA83 alloy with the addition of Ce.

3.2.2. Analysis of the hardness of as-soluted LA83 and LA83-1Ce alloys

Figure 12 plots the alloy-HV, α-HV and β-HV of the solution treated Mg-8Li-3Al-xCe($x = 0, 1.0$) alloys. For LA83 alloy, with the increase of solution time, the alloy-HV, α-HV and β-HV of alloys attain maximum values within 2 h. For LA83-1Ce alloy, with the increase of solution time, the alloy-HV and β-HV of alloys attain the maximum value within 2 h. The strengthening effect of β-HV is obviously better than that of the alloy-HV. At solution process, the strengthening rate of LA83 of alloy-HV is higher than that of LA83-1Ce alloy. This may be attributed to the solution strengthening effect weakening and the uneven distribution of AlCe and Al_2Ce phases. In a given range, the increase of solution time can increase the solid solubility of Al and Li in the matrix, which leads to increasing the HV of β phase of the two kinds of alloys greatly. With the increase of solution time, compounds in α-β boundaries regions are solutionized into α phase that results in the increase of HV of α phase of the two kinds of alloys.

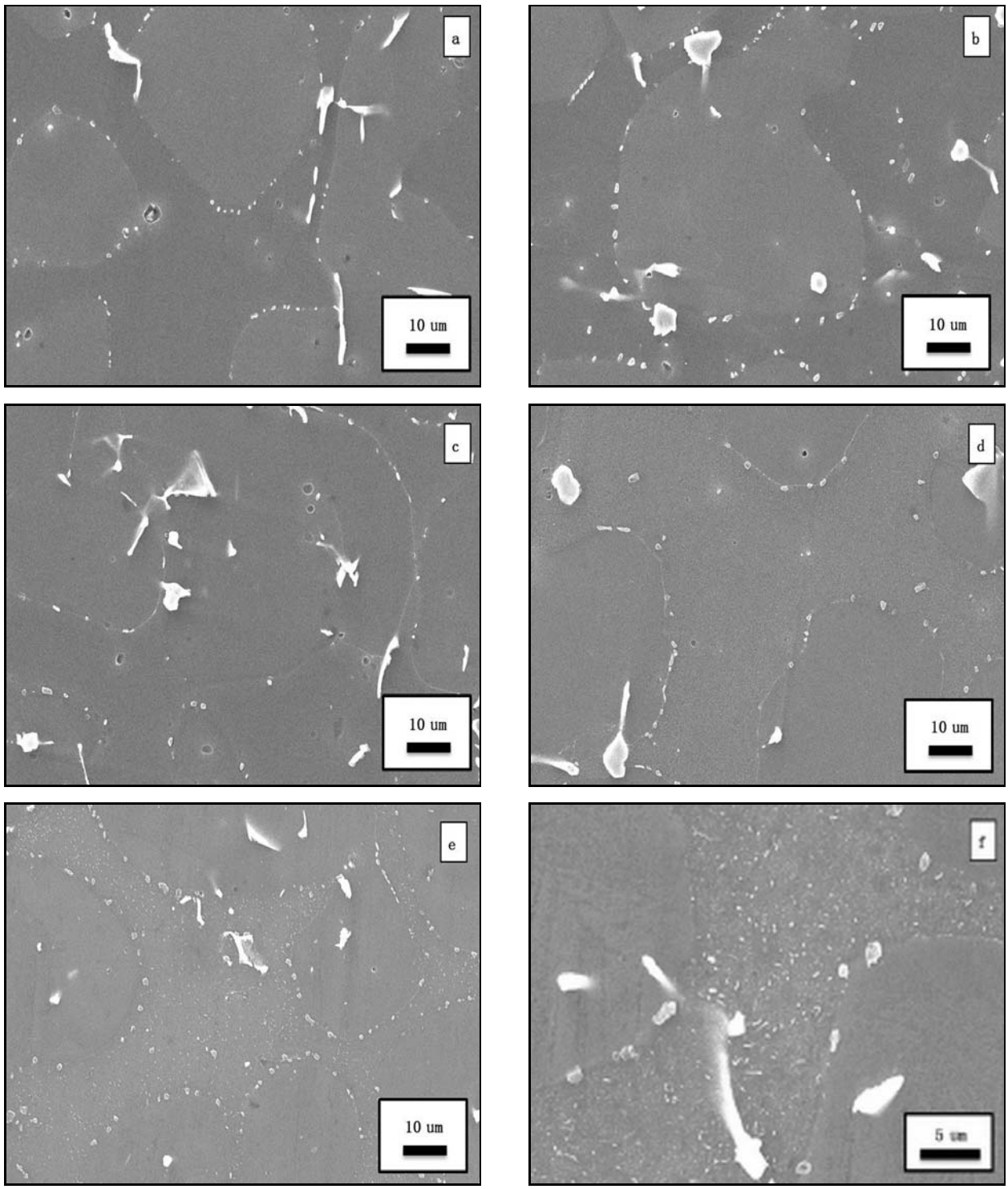

Fig. 9. SEM images of LA83-1Ce alloy aged for 1 h at different temperatures: (a) room temperature, (b) 50 ℃, (c) 100 ℃, (d) 150 ℃, (e) – (f) 200 ℃.

The highest HV of β phase of LA83 solution treated alloy is nearly as twice as that of LA83 as-cast alloy. When the content of Ce is 1 wt.%, the HV of β phase of each solution time is higher than solution treated LA83 alloys.

3.2.3. Comparison of the hardness of LA83 and LA83-1Ce aged alloys

Figure 13 shows aging curves of LA83-xCe(x = 0, 1.0) alloys aged for 1 h at different temperatures.

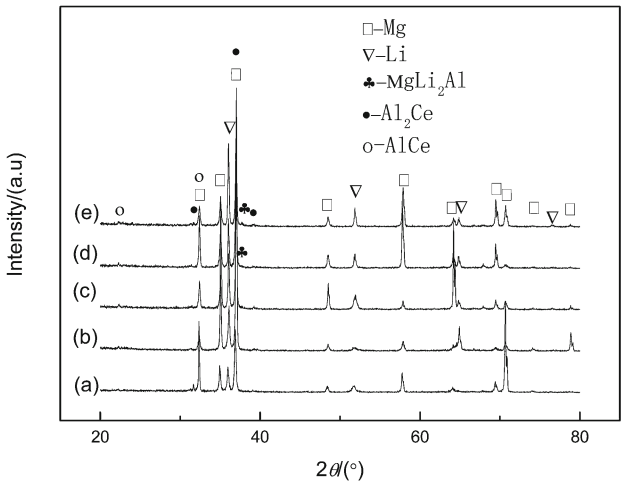

Fig. 10. XRD patterns of LA83-1Ce alloy aged for 1 h at different temperatures: (a) room temperature, (b) 50 ℃, (c) 100 ℃, (d) 150 ℃, (e) 200 ℃.

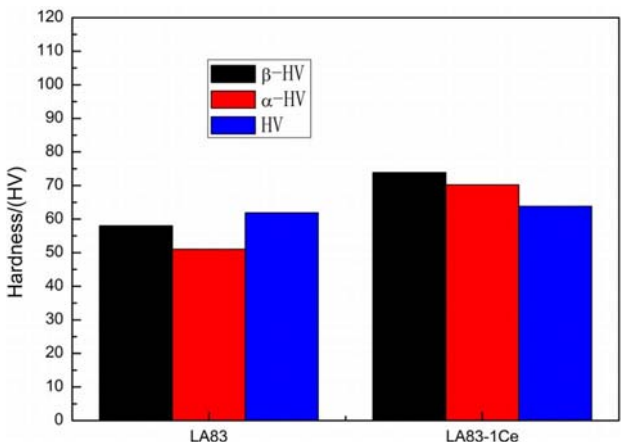

Fig. 11. The microhardness of studied as-cast alloys.

Age hardening for LA83-xCe(x = 0, 1.0) alloys could be observed for aging at 50 ℃. Moreover, LA83 and LA83-1Ce alloys show decrease in hardness for aging at temperatures higher than 100 ℃. Comparing the aging curves with XRD patterns and SEM images of LA83 aged alloy, the AlLi phase still exists and there is $MgLi_2Al$ phase precipitation when overage occurs. It comes to the conclusion that overage can be accounted for the weakening of solution strengthen. Therefore, during the aging process, the hardness of alloys increases first and then decreases with the aging temperature. When Ce element is added in alloys, the over aging process of β phase is retarded, which is attributed to the reduction of the amount of $MgLi_2Al$ precipitation. However, the α-HV values of the two alloys are unstable.

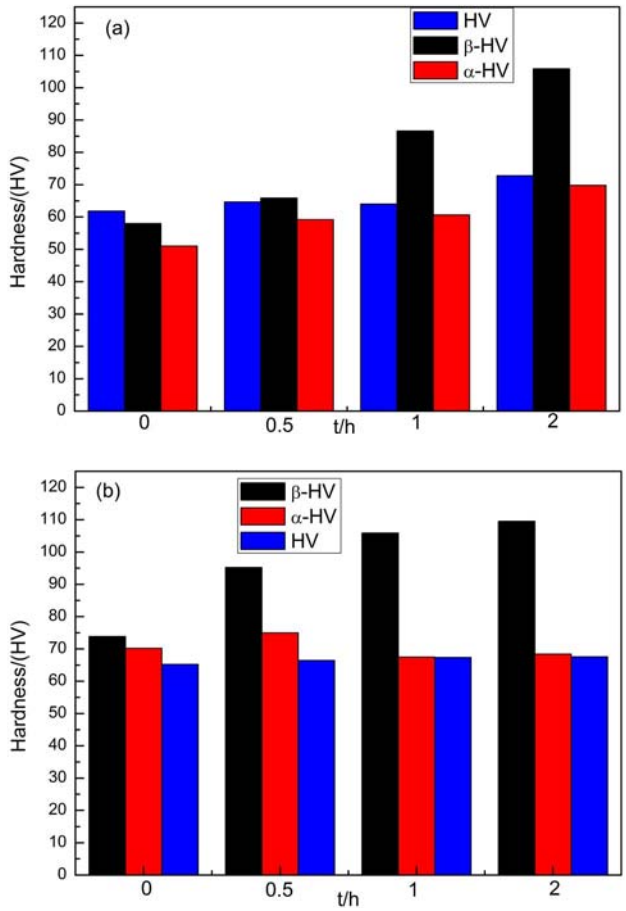

Fig. 12. Hardness of LA83-xCe alloys after solution treatment at 300 ℃ from 0 h to 2 h: (a) x = 0, (b) x = 1.

4. Conclusions

1. The as-cast LA83 alloy mainly consists of α-Mg, β-Li, AlLi and $MgLi_2Al$ phases. With the addition of Ce, AlLi phase disappears, the amount of $MgLi_2Al$ phase reduces, AlCe and Al_2Ce phases form. Moreover, the addition of Ce can refine and spheroidize the matrix. The as-cast LA83-1Ce alloy has relatively higher HV of α and β phases compared with LA83.

2. After solutionizing at 300 ℃ for 2 h, the $MgLi_2Al$ phases are completely solutionized into matrix, while the AlCe and Al_2Ce phases are not dissolved into the matrix. When LA83 alloy is solution treated at 300 ℃ for 2 h, fine lamellar AlLi phases precipitate in α phase.

3. When the solution time increases, it leads to an increase of the HV of β phase of the two kinds of alloys. When the content of Ce is 1 wt.%, β phase microhardness values of each solution time are higher than of solution treatment LA83 alloy.

4. LA83 and LA83-1Ce alloys show apparent aging phenomenon, especially for the LA83 alloy. $MgLi_2Al$

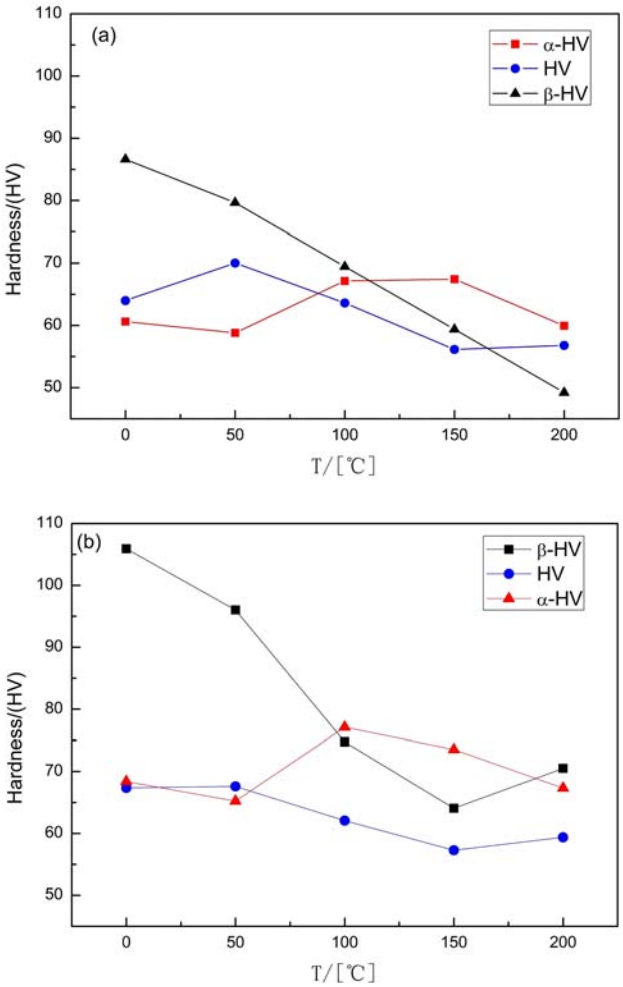

Fig. 13. Aging curves of LA83-xCe alloys aged for 1 h at different temperatures: (a) $x = 0$, (b) $x = 1$.

phase is identified in SEM image when LA83 alloy reaches its maximum hardness. It is concluded that this significant increase in hardness of the peak-aged alloy is due to the fine precipitated $MgLi_2Al$ phase particles by the peak-aging alloy at 50 ℃. However, there may be the possibility of change that is the transformation of AlLi phase to $MgLi_2Al$ phase. Nevertheless, the AlLi phase still exists and there is $MgLi_2Al$ phase precipitation when overage occurs. It comes to the conclusion that overage can be accounted to the weakening of solution strengthening.

Acknowledgements

This work was supported by the National Natural Science Foundation of China (51001034), Heilongjian Province Youth Skeleton Program (1252G018), Harbin City Innovative Talents Research Special Program (2012RFXXG094) and the Fundamental Research Funds for the Central Universities (HEUCF201310005).

References

[1] Sanschagrin, A., Tremblay, R., Angers, R., Dubé, D.: Mater. Sci. Eng. A, *220*, 1996, p. 69. doi:10.1016/S0921-5093(96)10460-3
[2] Chang, T. C., Wang, J. Y., Chu, C. L., Lee, S. Y.: Mater. Lett., *60*, 2006, p. 3272. doi:10.1016/j.matlet.2006.03.052
[3] Crawford, P., Barrosa, R., Mendez, J., Foyos, J., Es--Said, O. S.: J. Mater. Process. Technol., *56*, 1996, p. 108. doi:10.1016/0924-0136(95)01826-3
[4] Wu, L. B., Cui, C. L., Wu, R. Z., Li, J. Q., Zhan, H. B., Zhang, M. L.: Mater. Sci. Eng. A, *528*, 2011, p. 2174. doi:10.1016/j.msea.2010.11.063
[5] Chiu, C. H., Wu, H. Y., Wang, J. Y., Lee, S. Y.: J. Alloys Compd., *460*, 2008, p. 246. doi:10.1016/j.jallcom.2007.05.106
[6] Wu, S. K., Li, Y. H., Chien, K. T., Chien, C., Yang, C. S.: J. Alloys Compd., *563*, 2013, p. 234. doi:10.1016/j.jallcom.2013.02.073
[7] Kim, Y. W., Kim, D. H., Lee, H. I., Hong, C. P.: Scripta. Mater., *389*, 1998, p. 23.
[8] von Buch, F., Lietzau, J., Mordike, B. L., Pisch, A., Schmid-Fetzer, R.: Mater. Sci. Eng. A, *263*, 1999, p. 1. doi:10.1016/S0921-5093(98)01040-5
[9] Li, J. Q., An, J. M., Qu, Z. K., Wu, R. Z., Zhang, J. H., Zhang, M. L.: Mater. Sci. Eng. A, *527*, 2010, p. 7138. doi:10.1016/j.msea.2010.07.072
[10] Saito, N., Mabuchi, M., Nakanishi, M., Kubota, K., Higashi, K.: Scr. Mater., *36*, 1997, p. 551. doi:10.1016/S1359-6462(96)00420-4
[11] Wang, T., Zhang, M. L., Niu, Z. Y., Liu, B.: J. Rare Met., *24*, 2006, p. 797.
[12] Wang, J. Y.: J. Alloys Compd., *485*, 2009, p. 241. doi:10.1016/j.jallcom.2009.06.047
[13] McDonald, J. C.: J. Inst. Met, *97*, 1969, p. 353.
[14] Song, G. S., Staiger, M., Kral, M.: Mater. Sci. Eng. A, *371*, 2004, p. 371. doi:10.1016/j.msea.2004.01.017
[15] Wu, R. Z., Zhang, M. L.: Mater. Sci. Eng. A, *520*, 2009, p. 36. doi:10.1016/j.msea.2009.05.008
[16] Wu, H. Y., Lin, J. Y., Gao, Z. W., Chen, H. W.: Mater. Sci. Eng. A, *523*, 2009, p. 7. doi:10.1016/j.msea.2009.07.008
[17] Wang, T., Zhang, M. L., Wu, R. Z.: Mater. Lett., *62*, 2008, p. 1846. doi:10.1016/j.matlet.2007.10.017
[18] Alamo, A., Banchik, A. D.: J. Mater. Sci., *15*, 1980, p. 222. doi:10.1007/BF00552448
[19] Wu, H. U., Lin, J. Y., Gao, Z. W., Chen, H. W.: Mater. Sci. Eng. A, *523*, 2009, p. 7. doi:10.1016/j.msea.2009.07.008
[20] Wu, H. U., Gao, Z. W., Lin, J. Y., Chiu, C. H.: J. Alloys Compd., *474*, 2009, p. 158. doi:10.1016/j.jallcom.2008.06.145
[21] GB/T4340.1-2009. Measurement of Vickers hardness for metallic materials. Part I: experimental method. Standardization Administration of the People's Republic of China, 2009.
[22] Wu, L. B., Cui, C. L., Wu, R. Z., Li, J. Q., Zhan, H. B., Zhang, M. L.: Mater. Sci. Eng. A, *528*, 2011, p. 2174. doi:10.1016/j.msea.2010.11.063